Monthly Notices
of the
ROYAL ASTRONOMICAL SOCIETY

MNRAS **473,** 1589–1595 (2018)
Advance Access publication 2017 September 28

doi:10.1093/mnras/stx2506

Capture of free-floating planets by planetary systems

Nadav Goulinski★ and Erez N. Ribak★

Physics Department, Technion – Israel Institute of Technology, Haifa 32000, Israel

Accepted 2017 September 25. Received 2017 September 11; in original form 2017 May 26

ABSTRACT

Evidence of exoplanets with orbits that are misaligned with the spin of the host star may suggest that not all bound planets were born in the protoplanetary disc of their current planetary system. Observations have shown that free-floating Jupiter-mass objects can exceed the number of stars in our Galaxy, implying that capture scenarios may not be so rare. To address this issue, we construct a three-dimensional simulation of a three-body scattering between a free-floating planet and a star accompanied by a Jupiter-mass bound planet. We distinguish between three different possible scattering outcomes, where the free-floating planet may get weakly captured after the brief interaction with the binary, remain unbound or 'kick out' the bound planet and replace it. The simulation was performed for different masses of the free-floating planets and stars, as well as different impact parameters, inclination angles and approach velocities. The outcome statistics are used to construct an analytical approximation of the cross-section for capturing a free-floating planet by fitting their dependence on the tested variables. The analytically approximated cross-section is used to predict the capture rate for these kinds of objects, and to estimate that about 1 per cent of all stars are expected to experience a temporary capture of a free-floating planet during their lifetime. Finally, we propose additional physical processes that may increase the capture statistics and whose contribution should be considered in future simulations in order to determine the fate of the temporarily captured planets.

Key words: scattering – methods: numerical – methods: statistical – Planets and satellites: formation.

1 INTRODUCTION

The first notions of free-floating planets were brought about two decades ago through imaging observations (Tamura et al. 1998; Lucas & Roche 2000; Osorio et al. 2000). A decade later, the Microlensing Observations in Astrophysics (MOA) and Optical Gravitational Lensing Experiment (OGLE) groups conducted a gravitational microlensing survey towards the Galactic Bulge over two years (Sumi, Kamiya & Bennett 2011). They have estimated the population of free-floating planets to contain twice the number of main-sequence stars in our Galaxy.

The canonical planet formation mechanism is an *in situ* planet formation theory, dictating that planets form inside a protoplanetary disc. If so, planetary systems would have to be the only source of free-floating planets. An alternative suggestion adopts an *ex-situ* approach,[1] where Earth- to Jupiter-mass free-floating objects (hereafter referred to as 'free-floaters') may form by gravitational collapse of interstellar gas blobs. It has been suggested that high-speed gas blobs from the explosive death of stars may form free-floaters by accretion of interstellar ambient matter as they slow down and cool by radiation. Without an external source of heating, these cold and isolated gas blobs should collapse once they exceed Jeans mass (Dado, Dar & Ribak 2011). Such blobs and other filamentary structures are observed in large numbers in nearby supernova remnants (Fesen et al. 2006), planetary nebulae (O'Dell et al. 2002; Matsuura et al. 2009) or star formation regions, and are considered to be common in these stellar stages. Some of these blobs were observed as dense conglomerations of molecular clumps within H II regions (Haworth, Facchini & Clarke 2015), while other are ionized and metal-rich (Sahai, Scibelli & Morris 2016; Sato & Hughes 2017).

Measurements of the angle between the planetary orbital axis and the stellar spin axis (spin–orbit angle) reveal that a considerable fraction of the hot Jupiters have misaligned spin–orbit. This misalignment is at odds with the expectation of a close alignment between the spin of the star and the orbital motion of the planets, as they all should inherit their angular momentum from the protostellar disc. As for now, spin–orbit angles of 87 planets were calculated from light curves that exhibit anomalies due to the Rossiter–McLaughlin effect. About 40 per cent of them show significant spin–orbit misalignment, and nine of them are retrograde planets (Campante et al. 2016). There are several proposed mechanisms to resolve this problem, including multiple-planet scattering (Rasio et al. 1996; Beaugé & Nesvorný 2012), perturbations to

★ E-mail: nadavgs@campus.technion.ac.il (NG); eribak@physics.technion.ac.il (ENR)

[1] '*Ex-situ* formation' usually refers to planets formed in a different part of the protoplanetary disc. Here, we refer to the wider sense, formation outside the planetary system.

protoplanetary discs by gas captures (Bate, Lodato & Pringle 2010; Foucart & Lai 2011; Thies et al. 2011; Batygin 2012) and migration involving Lidov–Kozai oscillations (Correia et al. 2011; Naoz et al. 2013; Petrovich 2015; Anderson, Storch & Lai 2016; Storch, Lai & Anderson 2016). We suggest that captured free-floaters may account for some of these misaligned orbits, especially in regions of low velocity dispersion and with a large population of free-floaters.

Observations of supernova remnants and planetary nebulae each show thousands of blobs that can lead to considerable number densities of free-floaters, which may be large enough for captures to be common. A wide-field image of the Helix Nebula in the 2.12 μm molecular hydrogen line shows more than 40 000 low-mass blobs that constitute the only source of the H_2 surface brightness (Matsuura et al. 2009). If we assume that the only source of free-floaters are planetary nebulae and that the ∼40 000 blobs found in the Helix Nebula are a typical number for stars at this evolutionary stage, then a planetary nebulae number density of $\sim 5 \times 10^{-3}\,\mathrm{pc}^{-3}$ (Holberg, Oswalt & Sión 2002) predicts a blobs number density of $n_\mathrm{f} \approx 200\,\mathrm{pc}^{-3}$. In order to predict the capture rate of this kind of free-floaters by planetary systems, we evaluate the capture cross-section by simulating three-dimensional scatterings between a planetary-mass free-floater and a star-planet binary. This work is restricted to temporary captures, as we calculate the percent of brief interactions that bind the free-floaters, and for this purpose, we assume point mass objects and vacuum conditions. The dynamical evolution of the temporary captured free-floaters may involve tidal effects, gaseous environments and collisions with debris, for which dedicated simulations are required.

2 APPROACH

Significant orbit perturbations of a bound planet due to interactions with free-floaters are expected to occur for impact parameters of $-b_\mathrm{max} \le b \le b_\mathrm{max}$, where the value of b_max is determined by evaluating the maximal closest approach distance r_min from the host star, for which significant orbital perturbations are still possible. Let us assume that a free-floater with a relative velocity v_∞ at infinity is approaching a star-planet binary with an impact parameter b. Assuming that the mass of the star M is much larger then the mass of the bound planet m_B and the free-floater m_f, the trajectory of the free-floater is the one of a test-particle, and determined by the mass of the star. The cross-section for significant perturbations induced by this flux is the product of the geometrical area times the gravitational focusing factor

$$\mathcal{B} = \pi b^2 = \pi r_\mathrm{min}^2 \left(1 + \frac{2GM}{v_\infty^2 r_\mathrm{min}}\right). \tag{1}$$

We use an analytical expression for the closest approach r_min, that holds for $m_\mathrm{f}, m_\mathrm{B} \ll M$ (Donnison 1984)

$$r_\mathrm{min} = r_\mathrm{B} \frac{((1+\rho)^{\frac{3}{2}} - 1)^2}{2\rho^2}, \tag{2}$$

where r_B is the semimajor axis of the bound planet, and ρ is the mass ratio of the free-floater to the bound planet (hereafter the planetary-mass ratio).

We may write the differential size of the capture cross-section $\mathrm{d}\sigma$ as a product of the differential cross-section for a significant interaction $2\pi b \mathrm{d}b$ times the fraction of interactions that resulted in a capture P:

$$\mathrm{d}\sigma = P 2\pi b \mathrm{d}b. \tag{3}$$

The interaction cross-section depends on the relative velocity v, the mass of the host star M, the planetary-mass ratio ρ and the semimajor axis of the bound planet r_B; the last two determine the closest approach radius. The capture probability may also depend on similar variables, but dependence on relative velocity and the inclination angle is expected, since the perturbing impulse is affected.

Let us assume that a homogeneous flux of free-floaters with a given mass m_f, relative velocity v and a number density n_f is approaching with a given inclination angle θ_i at a planetary system. This flux will produce $n_\mathrm{f} v \mathrm{d}\sigma(v, \theta, M, r_\mathrm{min})/\mathrm{d}\Omega$ captures per second per solid angle. For a given relative velocity dispersion $\mathcal{S}$, the capture rate for a specific stellar mass and r_min is obtained by integrating with respect to velocity and over the full solid angle:

$$\mathrm{R}(M, r_\mathrm{min}) = \iint n_\mathrm{f} v \frac{\mathrm{d}\sigma(v, \theta, M, r_\mathrm{min})}{\mathrm{d}\Omega} f_\mathcal{S} \mathrm{d}v \mathrm{d}\Omega, \tag{4}$$

where $f_\mathcal{S}$ is the relative velocity distribution. The expected capture rate is obtained after integrating with respect to M and r_min according to their corresponding distribution function, and multiplying by the total number of stars N_stars:

$$\langle \mathrm{R} \rangle = N_\mathrm{stars} \int \mathrm{R}(M, r_\mathrm{min})\, f(M, r_\mathrm{min})\, \mathrm{d}M \mathrm{d}r_\mathrm{min}. \tag{5}$$

3 NUMERICAL METHOD

We follow the work of Varvoglis, Sgardeli & Tsiganis (2012), where they simulated scattering events of a Jupiter-mass free-floater by a binary of Sun-mass star and a Jupiter-mass planet. The free-floater was placed on a parabolic coplanar orbit and sufficiently far away to be considered as an unbound object. They mapped the resulting outcomes of the simulation for a grid of impact parameters b and initial orbital phases ϕ_B of the planetary system, and calculated the fraction of captures P. This is because different initial orbital phases lead to different impulse durations and strengths. It turned out that about 50 per cent of the initial condition grid led to a so-called 'temporary capture', where the fraction of captures that end up with moderate values of semimajor axis and eccentricity is in the order of 1 per cent. These captures are considered as temporary because simulating this isolated system for a large number of revolutions of the captured free-floater shows that most of them will eventually gain energy and escape. They also performed simulations for different free-floater masses, showing that the fraction of captures grows linearly with the mass, but not significantly.

The free-floater, as well as the host star and the bound planet, is set as a point-mass object. The masses of the star and the free-floater are simulation variables, while the mass of the bound planet is of one Jupiter mass. The bound planet is set to revolve around the host star on simple circular orbit. We define the inclination angle to be the one between the initial velocity vector of the free-floater v_f and the orbital axis of the bound planet (see Fig. 1). The initial distance of the free-floater from the system is set to be $r_0 = \sqrt{40 m_\mathrm{f}/m_\mathrm{B} r_\mathrm{B} + b^2}$, so that the initial binding energy between the free-floater and the binary is negligible. The corresponding initial velocity is obtained through conservation of energy

$$\frac{1}{2} m_\mathrm{f} v_\infty^2 = \frac{1}{2} m_\mathrm{f} v^2 - \frac{G m_\mathrm{f} (M + m_\mathrm{B})}{\sqrt{b^2 + (40 r_\mathrm{B})^2}}. \tag{6}$$

The simulations are carried for different masses of the free-floater and star, velocities and inclination angles. Each simulation run preforms multiple scattering that corresponds to a grid of impact parameters b and initial orbital phases of the bound planets ϕ_B. The

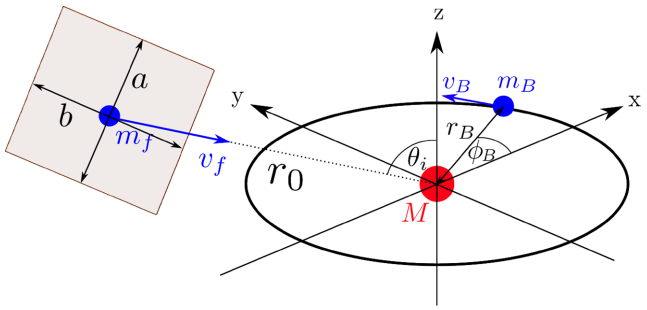

Figure 1. Schematic diagram of the scattering simulation. A free-floater (blue with the mass m_f) approaches a star-planet binary with a velocity of v_f and an inclination angle θ_i. The brown plane, which is orthogonal to the velocity vector, depicts the two components of the impact parameter $d = \sqrt{b^2 + a^2}$. Cases of $a \neq 0$ will be tested separately. The bound planet (blue with the mass m_B) revolves around the star (red with the mass M) on a circular orbit, with a radius of r_B and velocity $v_B = \dot{\phi}_B r_0$. The free-floater is placed at a distance of $r_0 \gg r_B$ from the y axis.

array of impact parameters b spans up to some maximal value b_{max}, for which significant perturbation may still occur (equation 2).

One may notice from Fig. 1 that all values of b lead for the path of the free-floater to intersect with the y-axis if no interaction with the bound planet took place. This means that the capture statistics that obtained from a simulation for some inclination angle θ_i do not necessarily predict the percentage of captures produced by a flux of free-floaters that passes through an area of πb^2. To account for this, the effect of a non-zero second component of the impact parameter, orthogonal to b and the velocity vector v_0, will be be tested separately.

The dynamical system is described by a simple Lagrangian. It includes the kinetic term of the two planets, the interaction term between them and their interaction terms with the star:

$$\mathcal{L}_{\rm kinetic} = \frac{1}{2} m_f v_f^2 + \frac{1}{2} m_B v_B^2, \tag{7}$$

$$\mathcal{L}_{\rm interaction} = G\frac{M m_f}{r_f} + G\frac{M m_B}{r_B} + G\frac{m_f m_B}{|\boldsymbol{r}_f - \boldsymbol{r}_B|}. \tag{8}$$

We do not add a kinetic term for the star since we assume standard planetary masses, for which the displacement of the star due to interaction is negligible down to red dwarf masses.

We preform the simulation for 175 values of $-b_{max} < b < b_{max}$ and 125 values of $0 < \phi < 2\pi$ for each inclination angle, velocity at infinity, mass of the free-floater and mass of the host star. The equations of motion are integrated until the free-floater travels out approximately twice its initial distance from the star. At this time, we calculate the sum of the kinetic and potential energy for two pairs: E_f – star and free-floater, and E_B – star and bound planet. The sign of the energy distinguishes between three outcomes, visualized in Fig. 2:

(i) Flyby: $E_f \geq 0$, $E_B < 0$
(ii) Capture: $E_f < 0$, $E_B < 0$
(iii) Exchange: $E_f < 0$, $E_B \geq 0$

The outcomes are saved together with their corresponding grid parameters (b, ϕ_B), for which the fraction of captures P is calculated.

In order to maximize the simulation speed, we used a grid resolution that is four times sparser then the one used by Varvoglis et al. (2012), but still high enough for statistical purposes. The numerical precision, however, must be sufficient enough so that the error in energy will be at least one order of magnitude smaller than the value itself. The numerical precision is set by two parameters: the first is the relative tolerance r_T, which determines the maximal relative error of the solution, and the second is the absolute tolerance a_T, which determines the last important digit of the solution. These parameters were set to $r_T = a_T = 10^{-7}$, for which the accuracy and the simulation speed are sufficient. We assume that the maximal error in every solution component y_i, taken as $|e_i| = r_T|y_i| + a_T$, has been achieved, so that the maximal error in E_f is

$$\delta E_f = \sqrt{\sum_i \left(\frac{\partial E_f}{\partial y_i}|e_i|\right)^2},$$

where $E_f = 1/2 m_f \dot{\boldsymbol{r}}^2 - m_f/r$. We calculate δE_f for every run of the simulation to assure that the number of runs that resulted with $\delta E_f/E_f > 0.1$ is less then 1 per cent.

4 RESULTS

We start with a Jupiter-mass free-floater that approaches the binary on a parabolic and coplanar orbit ($v_\infty = 0, \theta_i = 90^\circ$). The resulting outcome map is displayed in Fig. 3, where we use grey levels to distinguish between captures, flybys and exchanges. The grey area, which represents regions of b, ϕ_B values that led to captures, covers almost 50 per cent of grid. The upper an lower impact parameter values that were tested are those beyond which exchanges do not occur, indicating that significant orbital perturbations are no longer possible or too rare. Although statistically negligible, exchange events may also produce misaligned orbits, and they are considered as captures.

This outcome map agrees with the one presented by Varvoglis et al. (2012), implying the consistency of the method. Additionally, a variety of b, ϕ_B grid values with specific outcomes were selected from the map and tested individually to assure that the final energy

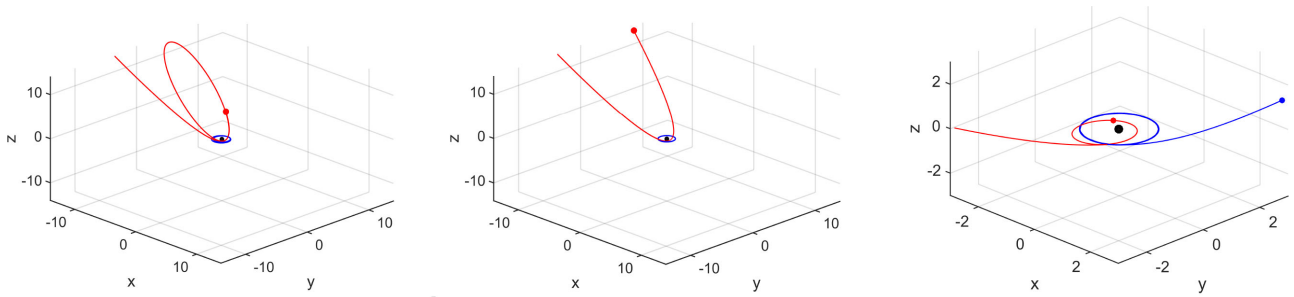

Figure 2. The interaction between the free-floater and the bound planet leads to three different possible outcomes of interest, which are displayed from the left- to right-hand side – a capture, a flyby and an exchange, where the free-floater 'replaces' the bound planet.

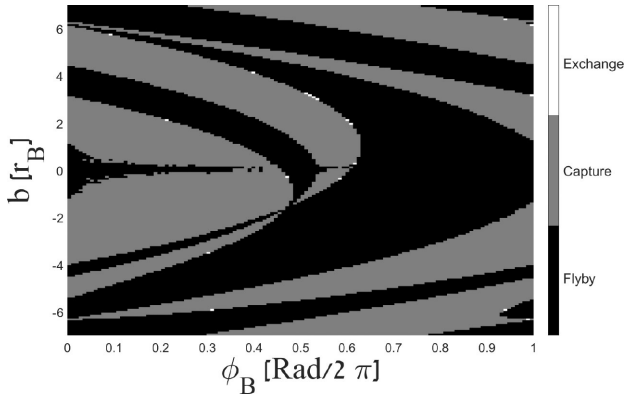

Figure 3. An outcome map for an inclination angle of $\theta_i = 90^\circ$, where the scatterings between the Jupiter-mass free-floater and a star-planet system are coplanar. Each point corresponds to a specific impact parameter b (175 in total) and an initial orbital phase of the bound planet ϕ_B (125 in total). An outcome where the free-floater remains unbound (flyby) is represented by a black colour, while the case where the free-floater gets captured is represented by a grey colour. Special cases where the free-floater 'kicks out' the bound planet and replaces it are seen as white dots on the boundary between the two main outcomes. The resulting capture probability is $P =$ 48.57 per cent.

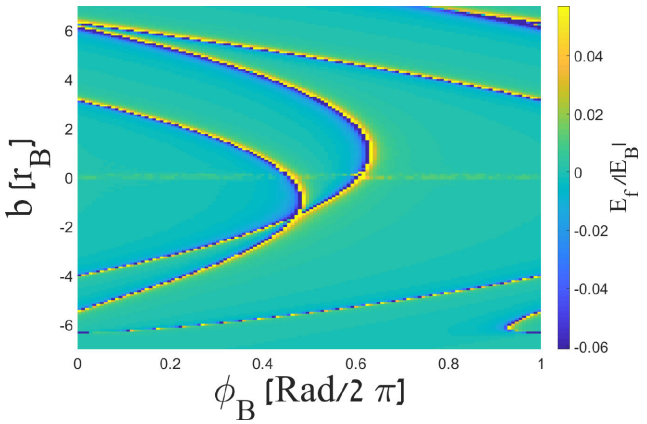

Figure 4. The final energy map of the free-floater, corresponding to Fig. 3. The colour spectrum represent the ratio between the final energy of the free-floater and the initial energy of the bound planet. The turquoise colour that covers most of the map represents energy ratio values that are very close to zero (the free-floater's original orbit is almost unaffected), while the yellow colour indicates flyby events with a significant excess of energy and blue colour indicates capture events with a significant negative energy (tightly bound). Values above 0.25 or below −0.25 were cropped.

values do not vary, and that the trajectories of the bodies agree with the outcomes.

The majority of the captures, however, end up with energies that are $\sim 10^{-3}$ time smaller then the initial energy of the binary, and are very eccentric and elongated. The outcome of the simulations is also plotted in Fig. 4 in terms of the ratio between the final energy of the free-floater and the initial energy of the binary. One can see that the maximal energy transfer takes place around the boundary between capture and flyby regions, at which exchange events are prone to happen. For most b, ϕ_B values, the total energy of the free-floater is almost unchanged. There is 'line' of significant positive energies around $b = 0$, where the minimal approach of the free-floater from the star is comparable to the numerical precision, and

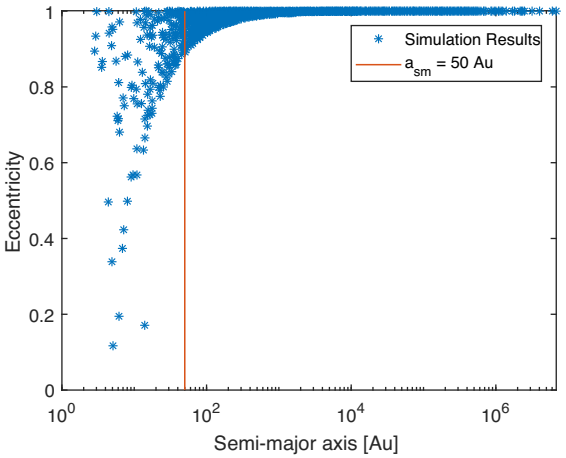

Figure 5. Eccentricity of the captured free-floaters as a function of the semi-major axis for a coplanar configuration and zero relative velocity at infinity. Only ∼0.9 per cent of the simulated captures ended up with a semimajor axis of $a_{sm} < 50$ au, which is marked by the vertical red line.

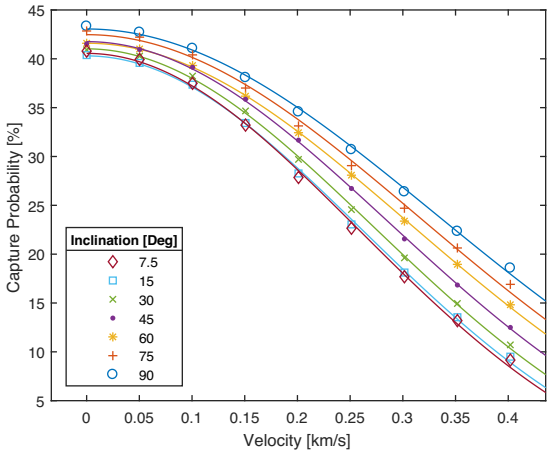

Figure 6. The dependence of the capture probability on the initial velocity at infinity of the free-floater. This dependence is plotted for different inclination angles of the star-planet system. The continuous curves represent the fitted Gaussian profiles, $P(v) = P_0 \exp(-v^2/2\Sigma^2)$.

deviation from conservation of energy becomes substantial. This small region is disregarded in the statistics.

The eccentricity as a function of the semimajor axis for the captured Jupiter-mass free-floaters is given in Fig. 5. Only ∼0.9 per cent of the simulated scattering events ended up with a semimajor axis of $a_{sm} < 50$ au, which is the distance of the Kuiper belt from the sun. According to our result, almost all free-floaters will reach their aphelion beyond the Kuiper belt if they would be captured by our Sun, but the number of $a_{sm} < 50$ au captures drops rapidly for slight deviations from coplanarity.

We cover a v_∞ initial velocity range for which the capture probability experiences significant variations. To evaluate the effect of the lateral impact parameter $a \neq 0$ on the statistics (Fig. 1), we ran additional simulations for a Jupiter mass free-floater with a fixed maximal value of $a = b_{max}$. The resulting statistics do not show dramatic variations in terms of capture probability, and they are averaged with the ones for $a = b_{max}$. Fig. 6 shows the dependence of the averaged capture probability on the velocity of the free-floater for all different inclination angels that were tested. The capture

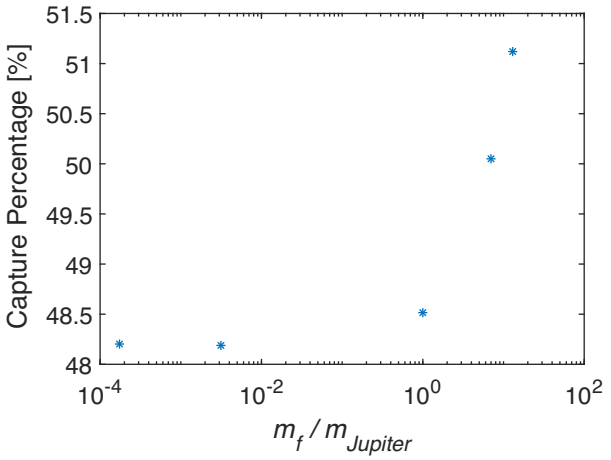

Figure 7. Capture percentage obtained from simulations of five different free-floater masses approaching the star-planet system at a coplanar configuration and zero initial velocity at infinity. The capture percentages obtained for $m_f = 7m_J$ and $m_f = 13m_J$ are slightly higher, but are still around 50 per cent.

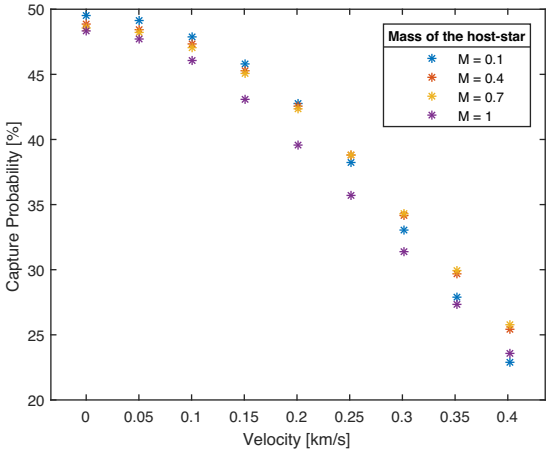

Figure 8. The dependence of the capture probability on the velocity of the free-floater at infinity, resulting from coplanar scattering simulations. Different colours represent different masses of the host star.

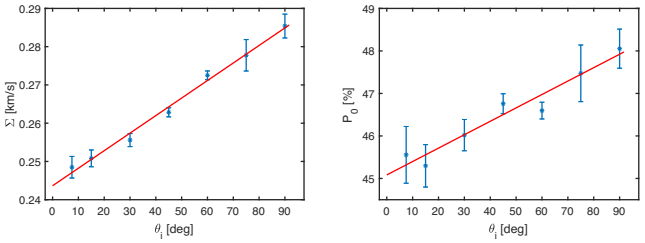

Figure 9. The dependence of the Σ and P_0 parameters on the inclination angle θ_i of the star-planet system, obtained by fitting the capture probability with $P(v) = P_0 \exp(-v^2/2\Sigma^2)$. The error bars mark the 95 per cent confidence level error range. The dependence was fitted with a simple linear function $f(\theta_i) = a\theta_i + b$ for both Σ and P_0. The parameter Σ is best fitted with $a = (0.53 \pm 0.5) \times 10^4\,\mathrm{cm \cdot s^{-1} \cdot rad^{-1}}$ and $b = (2.47 \pm 0.05) \times 10^4\,\mathrm{cm \cdot s^{-1}}$, while the best fit for P_0 is achieved with $a = 0.018 \pm 0.005$ and $b = 0.451 \pm 0.05$. The errors range is of 95 per cent confidence levels as well.

percentage is lower for free-floaters with higher initial velocity and lower inclination angle (towards a face-on inclination), which is expected since the orbital perturbation of the bound planet gets shorter. The resulting functionality is best fitted with a Gaussian $P(v) = P_0 \exp(-v^2/2\Sigma^2)$, where the parameter P_0 is capture fraction for the case of $v_\infty = 0$ and Σ is the standard deviation of the Gaussian profile.

To evaluate the dependence of the capture probability on the planetary-mass ratio, we preform a full simulation for two additional lighter free-floaters – Earth mass and Mercury mass and two additional coplanar scatterings for $7m_J$ and $13m_J$ free-floaters. The statistics for the different inclination angles and velocities hardly differed from the ones for Jupiter mass, and are effectively independent of the mass at this regime. The latter two exhibited a slight increase in the capture percentage, as displayed in Fig. 7.

The dependence of capture probability on the stellar mass is also needed to be analytically approximated. However, since 85 per cent of all stars are sub-solar, we performed additional coplanar scattering simulations with lower mass host stars to evaluate their effect. The resulting capture probabilities are shown in Fig. 8, and small differences of velocity dependence between the four tested masses can be noticed. This trend can be attributed to the shorter impulse that is needed for the free-floater to lose its energy. Still, assuming that this velocity dependence is best fitted with a Gaussian, the resulting standard deviations differ only by $\sim 0.3\,\mathrm{km\,s^{-1}}$. Since the typical velocity dispersion in our Galaxy is of the order of $\sim 10^2\,\mathrm{km\,s^{-1}}$, we do not expect the capture rate to be significantly affected.

5 THE CROSS-SECTION CONSTRUCTION

The fitted Gaussians profiles, shown in Fig. 6, predict the fraction of captures P for a given velocity. To account for the dependence on the inclination angle θ_i, we analyse the variations of the standard deviation Σ and the P_0 with the inclination angle, which are shown in Fig. 9.

We fit a linear function for both Σ and P_0, so that the capture probability, given in cgs units, is approximated analytically with $P(v, \theta_i) = (0.018\theta_i + 0.451)\exp[-v^2/10^8(0.75\theta_i + 3.5)^2]$. The orbital radius of the bound planet r_B was constant throughout the simulations, so a possible dependence of the capture probability on r_b is not accounted for; however, a Jupiter–Sun separation is indeed typical according to the NASA Exoplanet Archive.[2]

6 THE CAPTURE RATE

We evaluate the rate at which free-floaters get temporarily captured after a brief interaction with a star-planet binary. We restrict ourselves to the Galactic Thin Disc, which contains most of the stars in our Galaxy ($N_s \sim 10^{11}$), under the assumptions that each star is accompanied by a planet (Cassan et al. 2012). With a moderate typical velocity dispersion of $\sigma_v = 40\,\mathrm{km\,s^{-1}}$ and higher metallicity values, the thin disc may be considered as a plausible source of free-floaters and with higher capture rates (Murdin 2001). With a relative velocity dispersion of $\sigma_{rv} = \sqrt{2}\sigma_v$, we use a Boltzmann velocity distribution function for the region in question. The interaction cross-section that results for velocities lower than $v_{lim} = 0.07\,\mathrm{km\,s^{-1}}$ covers an area that is larger then the typical separation between the stars. To overcome this difficulty, we use a constant interaction cross-section of $\mathcal{B}_{lim} = n_{stars}^{-2/3} \simeq 3.7\,\mathrm{pc}^2$ for velocities below v_{lim}, where

[2] http://exoplanetarchive.ipac.caltech.edu/

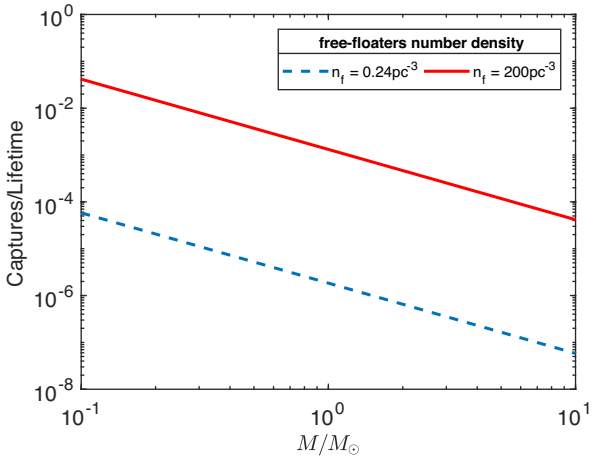

Figure 10. Expected stellar disc captures during the lifetime of the star as a function of the its mass. The red curve corresponds to the predicted free-floater's number density ($n_{\rm f}$) assuming that their origin is explosive death of stars, while the blue one corresponds to a free-floater's number density derived from microlensing surveys.

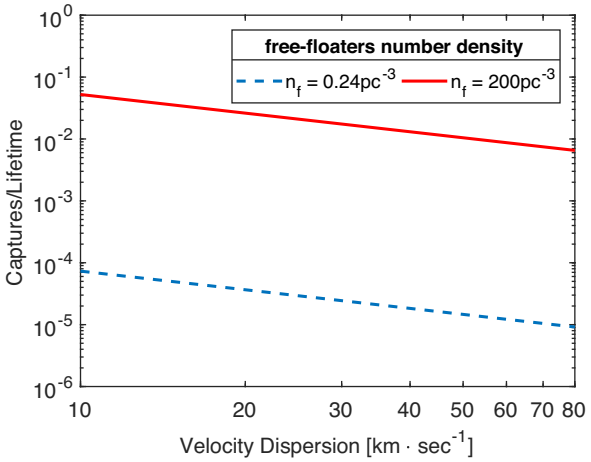

Figure 11. Percentage of stars that are expected to capture a free-floater during their lifetime as a function of the velocity dispersion. The red curve corresponds to the predicted free-floater's number density ($n_{\rm f}$) assuming that their origin is explosive death of stars, while the blue one corresponds to a free-floater's number density derived from microlensing surveys.

$n_{\rm stars} = 0.14\,{\rm pc}^{-3}$ is the number density of stars at the solar neighbourhood. This accounts for slow free-floaters that enter the unit volume of the star, while any free-floater outside of this volume is dominated by the gravity of another star. After integrating with respect to velocity and solid angle (equation 4), we obtain the capture rate as a function of the stellar mass and the planetary-mass ratio $\mathrm{R}(M, \rho)$.

We assume that a Jupiter mass is a typical mass of a free-floater, as predicted through observations by Sumi et al. (2011), and use the probability distribution function given by Malhotra (2015) for planetary masses. This distribution function is based on masses of observed Kepler exoplanets for which a debiased distribution was constructed. We also use a present-day mass function for the Galactic Thin Disc as presented by Chabrier (2003) and constructed from the observed luminosity function.

The number density of free-floaters $n_{\rm f}$ is assumed to be constant, as the density distribution of the free-floaters is yet unknown. Using a number density of $n_{\rm f} = 0.24\,{\rm pc}^{-3}$, as estimated by Sumi et al. (2011) from microlensing surveys, the capture rate in the Galactic Thin Disc is $R \simeq 6.4 \times 10^{-6}\,{\rm yr}^{-1}$ (equation 5), which is about one 'temporary capture' every 1.5×10^5 yr. If we adopt the *ex-situ* approach for the origin of free-floater as introduced by Dado et al. (2011), then a possible number density of $n_{\rm f} \approx 200\,{\rm pc}^{-3}$ is predicted, for which the capture rate in the Galactic Thin Disc is $R \approx 0.0046\,{\rm yr}^{-1}$; that is, we expect a 'temporary capture' to occur about every 218 yr.

The lifetime of stars varies according to their mass, due to fact that the mass is the energy source of the star and it dictates the energy output L (luminosity). A rough relation between the lifetime and mass is derived by evaluating the time required for the star to consume itself,

$$\tau\,(M) = \frac{f M c^2}{L} \sim \tau_{\odot} \left(\frac{M}{\mathrm{M}_{\odot}}\right)^{-2.5}, \qquad (9)$$

where $\tau_{\odot} = 10^{10}$ yr is the lifetime of the Sun. We use this estimation to evaluate the number of temporary captures that are expected for different stellar masses. As displayed in Fig. 10, it turns out that about one out of every ∼760 solar-mass stars is expected to experience capture a free-floater during its lifetime, while for red-dwarf stars with a mass of $0.1\,\mathrm{M}_{\odot}$, the expectancy is a capture by one out of every 25 stars.

As more then 85 per cent of the stars are of sub-solar masses, they are expected to be the main contributors to the capture rate. We estimate the expected fraction of stars that will capture a free-floater during their lifetime by calculating the expected value of $\mathrm{R}(M)\tau(M)$, where we use the initial stellar mass-function. We predict that ∼1 per cent of all $0.1\,\mathrm{M}_{\odot} < M < 2\,\mathrm{M}_{\odot}$ stars are expected to experience a capture during their lifetime.

The capture rate has a strong dependence on the velocity dispersion, as illustrated in Fig. 11, indicating that the majority of captures are expected to take place in very cold regions (i.e. of slow planets).

7 DISCUSSION

The vast majority of the capture events ends up with a very small binding energy between the free-floater and the host star, resulting in very elongated and eccentric orbits. Captured free-floaters may stay bound for a finite period of time until they gain energy back from planet–planet perturbation and get 'kicked out' back to the interstellar medium. The following perturbations can also cause the captured free-floater to lose energy and thus 'tighten' its orbit. Longer two-dimensional simulation carried by Varvoglis et al. (2012) showed that 90 per cent of the captured free-floaters eventually got ejected back to the interstellar medium. This result is in line with a direct proof by Littlewood (1952) that a non-dissipative three-body scattering event of point mass objects cannot produce a stable triplet. Such process is reversible and thus is analogous to a spontaneous ejection of a planet from a stable orbit. However, once introducing tidal effects and other possible dissipation mechanisms, the orbital evolution is no longer reversible. In most of our scattering simulations, the bound planet experienced only one perturbation, as the equations of motion were integrated up to the point where the free-floater travels about twice its initial distance.

The strong velocity dependence of the cross-section results in a very low capture rate of one capture every 218 yr in the Galactic Thin Disc, implying that captures are expected to occur in low-velocity dispersion regions. Moreover, we simulated low-velocity scatterings because captures are expected at this velocities range.

Since typical velocities in our Galaxy are much higher, scattering simulations at higher velocities are needed to avoid extrapolations.

Moreover, 42 per cent of the detected planetary systems contain more then one planet, and about one third of the stellar systems contain at least two stars. Simulating a planetary system with multiple bound planets should produce more boundaries between flyby and capture regions (see Figs. 4 and 3), at which significant orbit perturbations occur and hence increase the fraction of strong captures.

One must remember that our simulation assumed point masses and only the gravitational forces that they produce. We did not include any additional effects that may subtract energy from the interacting free-floater, such as tidal force and collision with clouds of debris; these should increase the capture fraction and tighten the orbits of captured planets. Not all captures, however, would be subjected to dissipation mechanisms in the same manner. Treating the eccentricity and the semimajor axis as additional variables of the cross-section would allow us to distinguish between captures that are too loose and inclined to remain bound, and those that might get tighter and circularized on reasonable time-scales. All these effects are left for future research.

A recent analysis of a large sample of microlensing events performed by Mróz et al. (2017) showed that the population of unbound Jupiter-mass planets is about ten times smaller then the one predicted by Sumi et al. (2011). Yet, a potential indication of the existence of Earth-mass and super-Earth-mass free-floating planets was found. Since microlensing events by lower mass lenses are harder to detect, many microlensing events by sub-Earth unbound planets could have been left undetected.

ACKNOWLEDGEMENTS

This work was partly supported by the Ministry of Science grant #880011. Additionally, this research has made use of the NASA Exoplanet Archive, which is operated by the California Institute of Technology, under contract with the National Aeronautics and Space Administration under the Exoplanet Exploration Program. We are very grateful for the useful comments of the reviewer, Joseph Antognini.

REFERENCES

Anderson K. R., Storch N. I., Lai D., 2016, MNRAS, 456, 3671
Bate M. R., Lodato G., Pringle J. E., 2010, MNRAS, 401, 1505
Batygin K., 2012, Nature, 491, 418
Beaugé C., Nesvorný D., 2012, ApJ, 751, 119
Campante T. L. et al., 2016, ApJ, 819, 85
Cassan A. et al., 2012, Nature, 481, 167
Chabrier G., 2003, PASP, 115, 763
Correia A. C., Laskar J., Farago F., Boué G., 2011, Celest. Mech. Dyn. Astron., 111, 105
Dado S., Dar A., Ribak E., 2011, ApJ, preprint (arXiv:1102.2622)
Donnison J., 1984, Celest. Mech., 32, 145
Fesen R. A. et al., 2006, ApJ, 645, 283
Foucart F., Lai D., 2011, MNRAS, 412, 2799
Goulinski N., Ribak E., 2016, Capture of Free-Floating Planets by Stellar Systems, The Israeli Physics Society Conference, Tel Aviv University
Haworth T. J., Facchini S., Clarke C. J., 2015, MNRAS, 446, 1098
Holberg J. B., Oswalt T. D., Sión E. M., 2002, ApJ, 571, 512
Littlewood J. E., 1952, On the problem of n bodies. Comm. Śem. Math. Unvi. Lund [Medd. Lunds Univ. Mat. Sem.], Tome Suppl´ementaire, p. 143
Lucas P., Roche P., 2000, MNRAS, 314, 858
Malhotra R., 2015, ApJ, 808, 71
Matsuura M. et al., 2009, ApJ, 700, 1067
Mróz P. et al., 2017, Nature, 548, 183
Murdin P., 2001, Encyclopedia of Astronomy and Astrophysics. IoP Publishing, Bristol, p. 3
Naoz S., Farr W. M., Lithwick Y., Rasio F. A., Teyssandier J., 2013, MNRAS, 431, 2155
O'Dell C., Balick B., Hajian A., Henney W., Burkert A., 2002, AJ, 123, 3329
Osorio M. Z., Béjar V., Martın E., Rebolo R., y Navascués D. B., Bailer-Jones C., Mundt R., 2000, Science, 290, 103
Petrovich C., 2015, ApJ, 799, 27
Rasio F. A., Ford E. B., 1996, Science, 274, 954
Sahai R., Scibelli S., Morris M., 2016, ApJ, 827, 92
Sato T., Hughes J. P., 2017, ApJ, 845, 167
Storch N. I., Lai D., Anderson K. R., 2016, MNRAS, 465, 3927
Sumi T., Kamiya K., Bennett D. P., 2011, Nature, 473, 349
Tamura M., Itoh Y., Oasa Y., Nakajima T., 1998, Science, 282, 1095
Thies I., Kroupa P., Goodwin S. P., Stamatellos D., Whitworth A. P., 2011, MNRAS, 417, 1817
Varvoglis H., Sgardeli V., Tsiganis K., 2012, Celest. Mech. Dyn. Astron., 113, 387

This paper has been typeset from a TEX/LATEX file prepared by the author.